with either the solution listed above (without ascorbic acid, *myo*-inositol, and Na-pyruvate) or a HEPES-based solution containing (in mM) 145 NaCl, 25 glucose, 2.5 KCl, 1 $MgCl_2$, 2 $CaCl_2$, 10 HEPES, bubbled with O_2 (used for Fig. 3a–c). During spillover experiments, the extracellular solution also contained 60 nM CGP54626 to prevent activation of $GABA_B$ receptors. Presynaptic terminals were labelled with lucifer yellow and visually identified as a calyx.

Electrodes for postsynaptic recording had resistances of 2–3 MΩ; series resistances during recordings were <5 MΩ, compensated electronically by 90%. Pre- and postsynaptic cells were voltage clamped to −60 mV, unless otherwise indicated. For presynaptic recordings, electrodes were 5–6 MΩ, with series resistances of 10–25 MΩ, compensated by 80–90%. Pipettes for recording EPSCs contained (in mM) 135 CsF, 5 CsCl, 5 EGTA, 10 HEPES and 2 QX314 (*N*-(2,6-dimethylphenylcarbamoylmethyl) triethylammonium chloride) (286 mOsm) at pH 7.25 with CsOH. Pipettes for pre- and postsynaptic recording of glycine responses contained either low $[Cl^-]_i$ solution (in mM): 125 Cs-methane sulphonate, 15 CsCl, 5 EGTA, 1 $MgCl_2$, 10 HEPES, 0.2 lucifer yellow (290 mOsm) at pH 7.2 with CsOH, or high-$[Cl^-]_i$ solution in which Cs-methane sulphonate was replaced with CsCl. Current-clamp recording from gramicidin-perforated patches was made with pipettes filled with high-$[Cl^-]_i$ solution where KCl replaced Cs-methane sulphonate and CsCl. For paired pre- and postsynaptic recordings, presynaptic pipettes contained (in mM) 150 KCl (or 145 K-gluconate and 5 KCl for low-$[Cl^-]_i$ solution), 0.2 EGTA, 1 $MgCl_2$ and 10 HEPES[13]. During simultaneous pre- and postsynaptic recordings, no rundown of EPSCs was observed over the 10–15 min necessary for the experiment. Voltages were corrected for junction potentials.

EPSCs and IPSCs were elicited by voltage pulses (100 μs, 10–20 V stimuli) delivered through a glass pipette. During paired pre- and postsynaptic recording, EPSCs were evoked by action potentials elicited by a depolarizing current pulse delivered through the presynaptic recording electrode. mEPSCs were recorded at −60 mV in the presence of 0.5 μM TTX. Drugs were applied by pressure ejection or by bath perfusion. Gramicidin D was prepared in methanol at 5 mg ml^{-1} and then dissolved in intracellular solution to a final concentration of 5 μg ml^{-1}. EGTA-AM prepared as a stock solution in dimethyl sulphoxide (DMSO) just before the experiment was diluted in bath solution to 0.2 mM (final concentration of DMSO, 0.1%). For Ca^{2+} measurements, voltage-clamped terminals were loaded with the presynaptic K-gluconate pipette fill containing 20 μM Oregon Green 488 BAPTA-1, and without Mg^{2+}. Dye was excited (Hg lamp with 1% neutral density filter, 470-nm bandpass excitation filter) at 1 Hz for 100 ms to minimize bleaching. Fluorescence emission (535 nm bandpass) was detected with a photomultiplier tube and was restricted to a region just larger than the cell body diameter. Background values, measured in a region of identical size adjacent to cell body, were subtracted and fluorescence changes normalized for the average pre-stimulus intensity ($\Delta F/F_0$). Statistical significance was established using paired and unpaired *t*-tests, as indicated, and errors reported as ±1 s.d.

Received 24 November 2000; accepted 27 March 2001.

1. Eccles, J. C., Schmidt, R. F. & Willis, W. D. Pharmacological studies of presynaptic inhibition. *J. Physiol.* **168,** 500–530 (1963).
2. Tachibana, M. & Kaneko, A. γ-Aminobutyric acid exerts a local inhibitory action on the axon terminal of bipolar cells: evidence for negative feedback from amacrine cells. *Proc. Natl Acad. Sci. USA* **84,** 3501–3505 (1987).
3. Zhang, S. J. & Jackson, M. B. $GABA_A$ receptor activation and the excitability of nerve terminals in the rat posterior pituitary. *J. Physiol. (Lond.)* **483,** 583–595 (1995).
4. Pouzat, C. & Marty, A. Somatic recording of GABAergic autoreceptor current in cerebellar stellate and basket cells. *J. Neurosci.* **19,** 1675–1690 (1999).
5. Forsythe, I. D. & Barnes-Davies, M. The binaural auditory pathway: excitatory amino acid receptors mediate dual timecourse excitatory postsynaptic currents in the rat medial nucleus of the trapezoid body. *Proc. R. Soc. Lond. B.* **25,** 151–157 (1993).
6. Taschenberger, H. & von Gersdorff, H. Fine tuning an auditory synapses for speed and fidelity during a critical developmental period. *J. Neurosci.* **24,** 9162–9173 (2000).
7. Bormann, J., Hamill, O. P. & Sakmann, B. Mechanism of anion permeation through channels gated by glycine and gamma-aminobutyric acid in mouse cultured spinal neurones. *J. Physiol. (Lond.)* **385,** 243–286 (1987).
8. Isaacson, J. S. $GABA_B$ receptor-mediated modulation of presynaptic currents and excitatory transmission at a fast central synapse. *J. Neurophysiol.* **80,** 1571–1576 (1998).
9. Takahashi, T., Kajikawa, Y. & Tsujimoto, T. G-Protein-coupled modulation of presynaptic calcium currents and transmitter release by a $GABA_B$ receptor. *J. Neurosci.* **18,** 3138–3146 (1998).
10. Martin, A. R. In *Handbook of Physiology, Sec. I, The Nervous System* (eds Brookhard, J. M., Mountscastle, V. B., Kandel, E. R. & Geiger, S. R.) 329–356 (Am. Physiol. Soc., Bethesda, 1977).
11. Atluri, P. P. & Regehr, W. G. Delayed release of neurotransmitter from cerebellar granule cells. *J. Neurosci.* **18,** 8214–8227 (1998).
12. Wang, L. Y. & Kaczmarek, L. K. High-frequency firing helps replenish the readily releasable pool of synaptic vesicles. *Nature* **394,** 384–388 (1998).
13. Borst, J. G. & Sakmann, B. Calcium influx and transmitter release in a fast CNS synapse. *Nature* **383,** 431–434 (1996).
14. Akaike, N. Gramicidin perforated patch recording and intracellular chloride activity in excitable cells. *Prog. Biophys. Mol. Biol.* **65,** 251–264 (1996).
15. Tachibana, M., Okada, T., Arimura, T., Kobayashi, K. & Piccolino, M. Dihydropyridine-sensitive calcium current mediates neurotransmitter release from bipolar cells of the goldfish retina. *J. Neurosci.* **13,** 2898–2909 (1993).
16. Cuttle, M. F., Tsujimoto, T., Forsythe, I. D. & Takahashi, T. Facilitation of the presynaptic calcium current at an auditory synapse in rat brainstem. *J. Physiol. (Lond.)* **512,** 723–729 (1998).
17. Borst, J. G. & Sakmann, B. Facilitation of presynaptic calcium currents in the rat brainstem. *J. Physiol. (Lond.)* **513,** 149–155 (1998).
18. Isaacson, J. S., Solis, J. M. & Nicoll, R. A. Local and diffuse synaptic actions of GABA in the hippocampus. *Neuron* **10,** 165–175 (1993).
19. Dittman, J. S. & Regehr, W. G. Mechanism and kinetics of heterosynaptic depression at a cerebellar synapse. *J. Neurosci.* **17,** 9048–9059 (1997).
20. Min, M. Y., Rusakov, D. A. & Kullmann, D. M. Activation of AMPA, kainate, and metabotropic receptors at hippocampal mossy fiber synapses: role of glutamate diffusion. *Neuron* **21,** 561–570 (1998).
21. Mitchell, S. J. & Silver, R. A. Glutamate spillover suppresses inhibition by activating presynaptic mGluRs. *Nature* **404,** 498–502 (2000).
22. Banks, M. I. & Smith, P. H. Intracellular recordings from neurobiotin-labeled cells in brain slices of the rat medial nucleus of the trapezoid body. *J. Neurosci.* **12,** 2819–2837 (1992).
23. Wu, S. H. & Kelly, J. B. Synaptic pharmacology of the superior olivary complex studied in mouse brain slice. *J. Neurosci.* **12,** 3084–3097 (1992).
24. Grothe, B. & Sanes, D. H. Synaptic inhibition influences the temporal coding properties of medial superior olivary neurons: an in vitro study. *J. Neurosci.* **14,** 1701–1709 (1994).
25. Funabiki, K., Koyano, K. & Ohmori, H. The role of GABAergic inputs for coincidence detection in the neurones of nucleus laminaris of the chick. *J. Physiol. (Lond.)* **508,** 851–869 (1998).
26. Schneggenburger, R. & Neher, E. Intracellular calcium dependence of transmitter release rates at a fast central synapse. *Nature* **406,** 889–893 (2000).
27. Bollmann, J. H., Sakmann, B. & Borst, J. G. Calcium sensitivity of glutamate release in a calyx-type terminal. *Science* **289,** 953–957 (2000).

Supplementary information is available on *Nature*'s World-Wide Web site (http://www.nature.com) or as paper copy from the London editorial office of *Nature*.

Acknowledgements

We thank S. Brenowitz, H. von Gersdorff and C. Jahr for comments on the manuscript. Supported by NIH grants and a Fogarty International Center Fellowship.

Correspondence and requests for materials should be addressed to L.T. (e-mail: trussell@ohsu.edu).

LTRPC7 is a Mg·ATP-regulated divalent cation channel required for cell viability

Monica J. S. Nadler*†, Meredith C. Hermosura*‡, Kazunori Inabe*§, Anne-Laure Perraud*†, Qiqin Zhu†, Alexander J. Stokes†, Tomohiro Kurosaki§, Jean-Pierre Kinet†, Reinhold Penner‡, Andrew M. Scharenberg†‖ & Andrea Fleig‡

† *Department of Pathology, Beth Israel Deaconess Medical Center and Harvard Medical School, Boston, Massachusetts 02215, USA*
‡ *Laboratory of Cell and Molecular Signaling, Center for Biomedical Research at The Queen's Medical Center and John A. Burns School of Medicine at the University of Hawaii, Honolulu, Hawaii 96813, USA*
§ *Department of Molecular Genetics, Institute for Liver Research, Kansai Medical University, Osaka 570-8506, Japan*
* *These authors contributed equally to this work*

The molecular mechanisms that regulate basal or background entry of divalent cations into mammalian cells are poorly understood. Here we describe the cloning and functional characterization of a Ca^{2+}- and Mg^{2+}-permeable divalent cation channel, LTRPC7 (nomenclature compatible with that proposed in ref. 1), a new member of the LTRPC family of putative ion channels. Targeted deletion of LTRPC7 in DT-40 B cells was lethal, indicating that LTRPC7 has a fundamental and nonredundant role in cellular physiology. Electrophysiological analysis of HEK-293 cells overexpressing recombinant LTRPC7 showed large currents regulated by millimolar levels of intracellular Mg·ATP and Mg·GTP with the permeation properties of a voltage-independent divalent cation influx pathway. Analysis of several cultured cell types demonstrated small magnesium-nucleotide-regulated metal ion currents (MagNuM) with regulation and permeation properties essentially identical to the large currents observed in cells expressing recombinant LTRPC7. Our data indicate that LTRPC7, by

‖ Present address: Department of Pediatrics and Immunology, University of Washington and Children's Hospital and Medical Center, Seattle, Washington 98195-6320, USA.

© 2001 Macmillan Magazines Ltd

virtue of its sensitivity to physiological Mg·ATP levels, may be involved in a fundamental process that adjusts plasma membrane divalent cation fluxes according to the metabolic state of the cell.

As part of a systematic effort to identify novel Ca^{2+}/cation channels expressed in haematopoietic cells, we cloned a putative cation channel transcript, which we later designated LTRPC7. The predicted protein encoded by the LTRPC7 transcript is homologous to other LTRPC family members throughout its first 1,200 amino acids (Fig. 1a), but is notable for its ubiquitous distribution (see Supplementary Information) and for a long and unique carboxy-terminal tail that contains a domain of significant homology to the MHCK/EEF2α family of protein kinases[2] (Fig. 1a).

To investigate LTRPC7's role in cell physiology, we used the DT-40 B-cell system to produce a cell line with targeted deletion of its LTRPC7 genes. Although targeted deletion of one LTRPC7 allele was easily obtained, no clones were obtained with targeted integrations into both alleles (data not shown), indicating that LTRPC7 is required for cellular viability. We therefore took an inducible deletion approach (Fig. 1b) by producing a viable DT-40 cell line that expressed a tamoxifen-controlled Cre recombinase, and which also had a stable targeted deletion of one LTRPC7 allele and LoxP sites bracketing the LTRPC7 exons encoding transmembrane span 5, the putative channel pore region and transmembrane span 6 in the other LTRPC7 allele. Activation of the Cre recombinase by treatment of this cell line with tamoxifen induced the deletion of these three exons in most cells (Fig. 1c). As shown in Fig. 1d, this induced the growth arrest and subsequent death of the cells over a 48–72-h time frame, providing strong evidence that LTRPC7 is fundamental in cellular function.

For electrophysiological analysis of LTRPC7, we produced HEK-293 cell lines with tetracycline-controlled expression of a Flag-tagged LTRPC7 construct. Treatment of these cells with tetracycline for 24 h induced a Flag-reactive band with a relative molecular mass of 220,000 (M_r 220K; predicted size of Flag–LTRPC7, Fig. 2a). However, by 72–96 h, LTRPC7-expressing cells began to swell, detach and die (Fig. 2b, similar results for all clones). Because of the potential for cell toxicity at times greater than 24 h after induction, all subsequent analyses were performed 18–24 h after induction. In this time frame, induced cells developed large whole-cell currents over a 100–300-s time period (Fig. 2c) with a characteristic outwardly rectifying current–voltage relationship (Fig. 2d) when perfused with Cs^+-based internal solutions (identical results were obtained with K^+, data not shown). With choline-based intracellular solutions, the large outward conductances were significantly suppressed, indicating that outward currents through LTRPC7 are carried by cations. Stationary noise analysis of outward currents was performed at +60 mV in the frequency range 0.001–1 kHz and revealed characteristic increases in current variance during activation of the whole-cell current that levelled off and finally decreased as the current was fully activated. Through linear regression of variance versus mean current during the initial activation phase, we determined an average slope of 2.5 ± 0.4 pA (n = 4), corresponding to a single-channel conductance of ~40 pS, based on a reversal potential of 0 mV. Because mono- and divalent ions do not permeate LTRPC7 independently of each other (see below), this value applies in a strict manner only to the test potential of +60 mV and the ionic conditions imposed by our external and internal solutions.

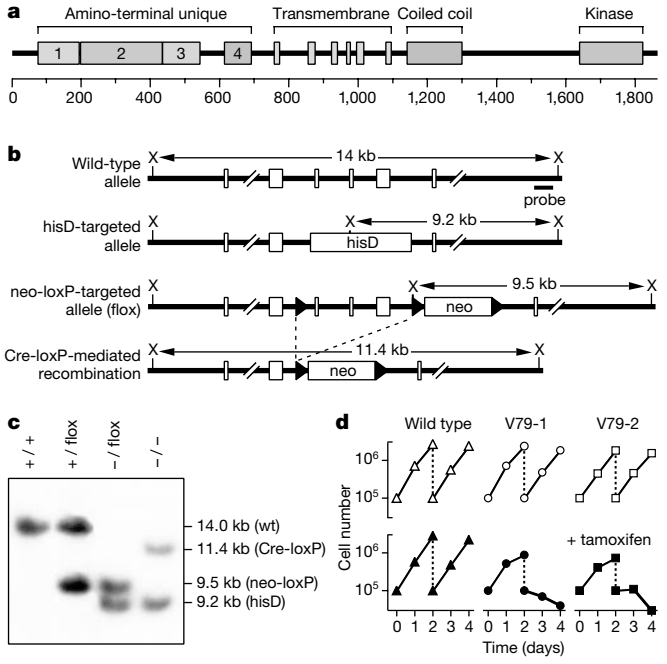

Figure 1 LTRPC7 structure and inducible knockout of LTRPC7 in the chicken B-cell line DT-40. **a**, Schematic of LTRPC7 with amino-terminal unique regions 1–4, transmembrane domain regions, coiled-coil region and the MHCK/EEF2α kinase homology domain (kinase). **b**, Schematics of wild-type and mutated DT-40 LTRPC7 alleles. Restriction enzyme sites (X, *Xba*I), probe for Southern blot analysis (solid bar), exons (open rectangle) and loxP sites (solid triangle) are indicated. Three exons, including part of the putative transmembrane region (corresponding to mouse LTRPC7 amino-acid residues 997–1,158), were replaced with *hisD* cassettes in the *hisD*-targeted allele and flanked by two *loxP* sequences in the *neo-loxP*-targeted allele. *Xba*I fragments detected by the probe are shown for wild-type and mutated alleles. **c**, Southern blot analysis of *Xba*I-digested DNA from wild-type and mutant DT-40 cells. **d**, Effect of LTRPC7 inactivation on cell proliferation. DT-40 wild type and mutant clones (V79-1 and V79-2) harbouring *hisD*- and *neo-loxP*-targeted alleles were cultured either without (open symbols) or with (filled symbols) 200 nM tamoxifen. Cell numbers were adjusted to 1×10^5 cells per ml, 2 days after cultivation. Viable cells were monitored daily by trypan blue exclusion.

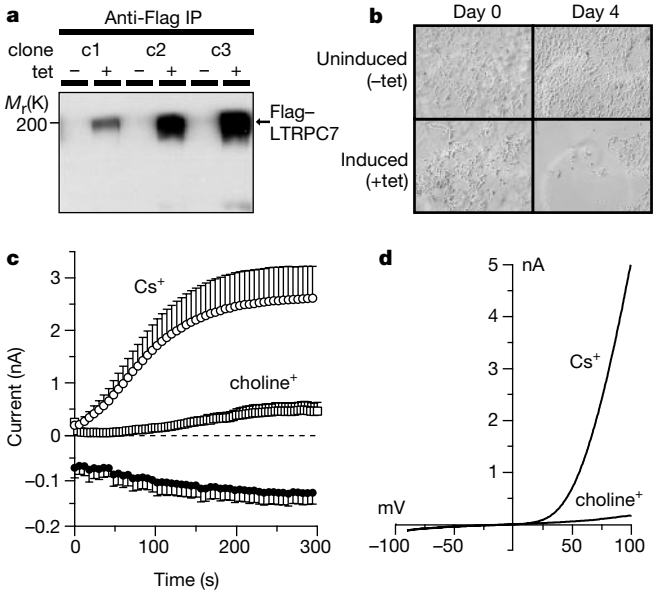

Figure 2 Functional expression of LTRPC7 as a cation channel**. a**, SDS–polyacrilamide gel electrophoresis (PAGE) analysis of three clonal HEK-293 cell lines (c1–c3) expressing a tetracycline-controlled Flag–LTRPC7 construct. Anti-Flag immunoreactive proteins before (left lanes) or after 24 h of tetracycline (right lanes). **b**, Phase contrast images of representative patches of LTRPC7-overexpressing HEK-293 cells 0 and 4 days after treatment with or without tetracycline. **c**, Average inward and outward currents carried by LTRPC7 at –80 and +80 mV, respectively. Cells perfused with ATP-free Cs^+-glutamate internal solution (n = 7, ± s.e.m.). Outward current was markedly suppressed when choline was used as the major internal cation, with only 10 mM Cs^+ present (n = 3, ± s.e.m.). **d**, Current–voltage relationships under experimental conditions as in **c**, obtained from representative cells 200 s after whole-cell establishment.

© 2001 Macmillan Magazines Ltd

We next analysed the permeation characteristics of LTRPC7-mediated currents (Fig. 3). Inward currents were not affected by substitution of choline for Na^+ and K^+ in the extracellular solution (Fig. 3a), indicating that the inward current is carried exclusively by divalent ions. Furthermore, inward currents are not affected by removal of either Ca^{2+} or Mg^{2+} alone (Fig. 3b, c). Only the complete removal of external divalents amplifies both inward and outward monovalent current flow (Fig. 3d). The current–voltage relationship under divalent-free conditions (Fig. 3e) demonstrates linearization of the outward currents and significant enhancement of inward currents as compared with the divalent-containing situation. These effects are probably due to relief from permeation block by the divalent ions, which is expected to be strongest at negative potentials and gradually decreases as the reversal potential for divalent ions is approached.

The above data are most simply explained by a model in which the LTRPC7 pore has a high affinity for and is permeant to $Ca^{2+}$and Mg^{2+}, which accordingly obstruct inward fluxes of monovalent cations. Consistent with this model, LTRPC7-dependent inward currents are enhanced and outward currents suppressed when cells are exposed to isotonic (120 mM) $CaCl_2$ and $MgCl_2$ solutions, conditions in which Ca^{2+} or Mg^{2+} are the only available cationic charge carriers (Fig. 3f and g, respectively). In light of the significant Mg^{2+} permeation of LTRPC7, a feature to our knowledge unprecedented among known ion channels, we assessed Mg^{2+} permeation at different extracellular Mg^{2+} concentrations in reference to inward currents carried by 2 mM Mg^{2+} (Fig. 3h; note the absence of external Ca^{2+}). Higher concentrations of Mg^{2+} increased inward currents carried by Mg^{2+} and submillimolar Mg^{2+} concentrations progressively increased monovalent influx until divalent-free medium gave rise to large monovalent inward currents. Thus, LTRPC7 exhibits clear Mg^{2+}-dependent anomalous mole fraction behaviour. At the same time, outward currents are inhibited with increasing Mg^{2+} concentrations (Fig. 3i), probably in part owing to the shift in reversal potential occurring with the increase in extracellular Mg^{2+} concentrations, but also indicating that Mg^{2+} upon permeation might suppress LTRPC7 intracellularly (see below).

The time course of passive activation of currents carried by LTRPC7 is most consistent with activation due to diffusional depletion of a small intracellular constituent that suppresses channel opening. On the basis of the results above and the presence of the α-kinase domain in LTRPC7, we suspected that $[Mg^{2+}]_i$ and $[ATP]_i$ might be involved in LTRPC7 regulation. We therefore systematically changed the $[Mg^{2+}]_i$ and $[ATP]_i$ of our patch pipette solutions. LTRPC7 channel activity is strongly suppressed by Mg·ATP concentrations in the millimolar range (Fig. 4a, d), with nearly complete suppression of currents at 6 mM Mg·ATP. Under these conditions, free $[Mg^{2+}]_i$ varies from 670 to 800 μM, and the available ATP is essentially all in the physiological Mg·ATP form. However, no suppressive effect is observed when 2 mM Na·ATP is added to a $[Mg^{2+}]_i$-free internal solution, weighing against a role for a standard high-energy phosphate group transfer in the suppression phenomenon as well as indicating that $[Mg^{2+}]_i$ is a required factor or cofactor for inhibition. Figure 4b summarizes the average currents observed during intracellular perfusion of cells with solutions devoid of ATP but containing different free Mg^{2+} concentrations. From this, it is evident that high $[Mg^{2+}]_i$ strongly suppresses LTRPC7-dependent currents even in the absence of ATP, with 3 mM causing a complete block (Fig. 4e).

To evaluate further the potential role of high-energy phosphate transfer in suppression, we perfused cells with four different Mg^{2+}-nucleotide trisphosphates (NTP) to define the nucleotide specificity (Fig. 4c). At 2 mM (free $[Mg^{2+}]_i \approx 700–850$ μM), both ATP and GTP largely suppressed activation of LTRPC7 currents (with essentially identical dose–response curves), whereas CTP and ITP were less effective compared with NTP-free controls. If the dose–

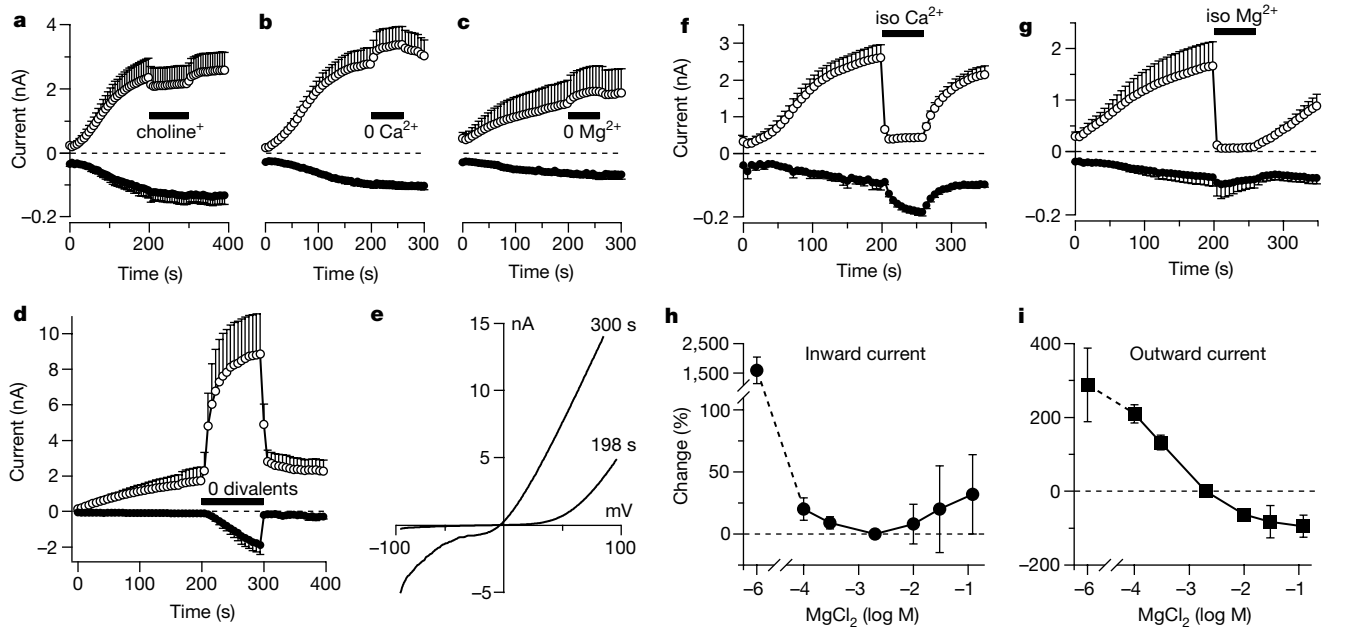

Figure 3 Permeation and block of LTRPC7 by divalent ions. Average inward and outward currents carried by recombinant LTRPC7 at −80 and +80 mV, respectively. Black bars indicate solution changes. **a**, Extracellular solutions contained 10 mM Ca^{2+} and 2 mM Mg^{2+}. Inward currents remained unaffected by application of extracellular solution in which NaCl was replaced by choline-Cl ($n = 5$). **b**, Application of Ca^{2+}-free extracellular solution ($n = 5$). **c**, Application of Mg^{2+}-free extracellular solution ($n = 5$). **d**, Removal of both Ca^{2+} and Mg^{2+} ($n = 5$). **e**, *I–V* relationship of currents under conditions as in **d** elicited before divalent-free application (198 s) and just before re-admission of divalents (300 s). **f**, **g**, Application of isotonic $CaCl_2$ or $MgCl_2$ (120 mM) reversibly enhanced inward currents and strongly inhibited outward currents ($n = 5$ each). **h**, Anomalous mole fraction behaviour of Mg^{2+} permeation. Changes in inward current measured at −80 mV as a function of extracellular Mg^{2+} concentration ($n = 3–5$; Mg^{2+}-free solution plotted at 1 μM) and normalized in reference to 2 mM extracellular Mg^{2+} (extracellular solutions were nominally Ca^{2+}-free). **i**, Analysis of the corresponding changes in outward currents (measured at +80 mV) in the same cells as in **g** (also in reference to 2 mM Mg^{2+}).

© 2001 Macmillan Magazines Ltd

response curve for ATP (Fig. 4d) is instead plotted as a function of calculated free $[Mg^{2+}]_i$ (Fig. 4e, open boxes), it can be seen that suppression of LTRPC7 currents by Mg·ATP occurs within a range of free $[Mg^{2+}]_i$ that produces only moderate suppressive effects on LTRPC7 in the absence of ATP or GTP (Fig. 4e, filled circles). Together, these results would be most consistent with Mg·ATP acting as a physiological regulator of LTRPC7, as cellular levels of free $[Mg^{2+}]_i$ are around 0.5 mM (ref. 3) and cytosolic GTP levels are at least five times lower than those of ATP, which are typically several millimolar[4].

Finally, as a further test of a role for a high-energy phosphate transfer reaction in LTRPC7 gating, we performed experiments with Na·ATP-γ-S and Mg·ATP-γ-S, non-hydrolysable analogues of ATP. Because ATP-γ-S can be used by protein kinases in thio-phosphorylation reactions, and thio-phosphate linkages are not susceptible to protein phosphatases, the result is irreversible protein phosphorylation. As shown in Fig. 4f (open diamonds), 2 mM Mg·ATP-γ-S (free $[Mg^{2+}]_i \approx 700\ \mu M$) effectively suppresses LTRPC7 currents. To address the question of whether this suppression is due to irreversible thio-phosphorylation of LTRPC7, we performed experiments in which cells were initially patched with pipette solutions containing Mg·ATP-γ-S (filled circles in Fig. 4f) and subsequently re-patched around 180 s later, this time with an ATP-free pipette solution to wash out Mg·ATP-γ-S. This resulted in essentially full re-development of LTRPC7 currents, demonstrating the reversibility of the suppression phenomenon under conditions in which the participation of a phosphorylation event should have resulted in irreversible suppression. Therefore, the suppression of LTRPC7 activation by Mg·ATP-γ-S is analogous to that of Mg·ATP or Mg·GTP and is likely to be the result of direct regulation of channel activity. By the same logic, Na·ATP-γ-S should behave similarly to Na·ATP and this is confirmed in Fig. 4f (open circles), where 2 mM Na·ATP-γ-S failed to suppress LTRPC7 activation. We did observe a Na·ATP-γ-S-mediated delayed and slow inactivation, which may involve phosphorylation events that downregulate LTRPC7 activity.

We also analysed endogenous currents activated in several cultured cell lines from tissues positive for LTRPC7 transcripts, using the same experimental conditions that produced maximal LTRPC7 activation in our heterologous HEK-293 system. Each cell type analysed (Fig. 5) possessed currents with Mg·ATP sensitivity and current–voltage relationship similar to those observed in HEK-293 cells overexpressing LTRPC7. In particular, the native currents exhibited strong outward rectification at potentials above +50 mV, which may be considered the signature of this conductance. We have adopted the convention that native currents that exhibit sensitivity to Mg·nucleotide complexes and permeation properties like those of LTRPC7 are designated as magnesium·nucleotide-regulated metal ion currents or MagNuM. Our data indicate that LTRPC7 mediates most or all of MagNuM in all cell types so far analysed.

An analysis of LTRPC7 function has also been performed by Clapham and colleagues[5]. They concluded that the EEF2α domain kinase activity was required for channel gating. However, this conclusion was based in part on increased currents observed upon addition of 5 mM Na·ATP to a standard intracellular solution containing only 1 mM $MgCl_2$, reducing free $[Mg^{2+}]_i$ to 6 μM. As our data show Mg^{2+} to be an essential (co)factor in regulating LTRPC7 activity, such a drop in free $[Mg^{2+}]_i$ would be expected to produce a large relative increase in current amplitude independent of ATP, suggesting that conclusions regarding the role of the kinase domain in channel activation should be taken cautiously. Clapham and

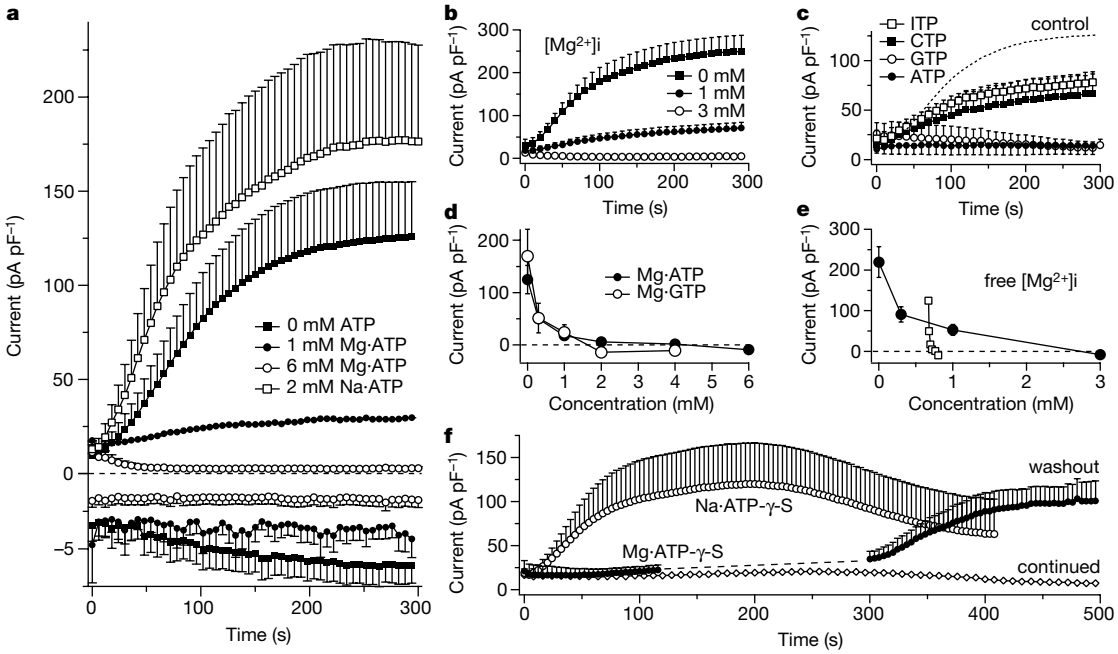

Figure 4 LTRPC7 gating is modulated by $[Mg^{2+}]_i$ and Mg·nucleotides. **a**, Average inward and/or outward currents carried by recombinant LTRPC7 at –80 and +80 mV, respectively. Cells were perfused with internal solutions containing various ATP concentrations (0 mM Mg·ATP, $n = 7$; 1 mM Mg·ATP, $n = 5$; 6 mM Mg·ATP, $n = 5$; 2 mM Na·ATP, $n = 5$). **b**, Cells were perfused with internal solutions containing the indicated $MgCl_2$ concentrations in the absence of added ATP (in all cases $n = 5$). **c**, Cells were perfused with internal solutions containing 2 mM of various Mg·nucleotides (in all cases $n = 5$). Dotted control trace represents 0 ATP taken from **a**. **d**, Average changes of maximum outward current measured at +80 mV as a function of intra-pipette Mg·ATP or Mg·GTP levels. The change in current size was analysed by subtracting the first data trace acquired after whole-cell establishment from the one elicited at 300 s. **e**, Average changes of maximum outward current measured at +80 mV as a function of intra-pipette free Mg^{2+} levels in the absence of added ATP (filled circles). The change in current size was analysed as in **d**. Open squares, data points of the ATP dose–response curve in **d**, here plotted against the calculated free Mg^{2+} under those conditions. **f**, Cells were perfused with internal solutions containing 2 mM of various non-hydrolysable analogues of ATP (Na·ATP-γ-S, open circles, $n = 6$; Mg·ATP-γ-S, open diamonds, $n = 3$). Filled circles represent three cells perfused with 2 mM Mg·ATP-γ-S for 120 s and then re-patched with ATP-free solution. Data sets from re-patched cells were aligned, averaged and plotted with a delay of 180 s, which represents the average time needed to exchange pipettes and re-patch individual cells (120 s, 198 s, 215 s, respectively).

© 2001 Macmillan Magazines Ltd

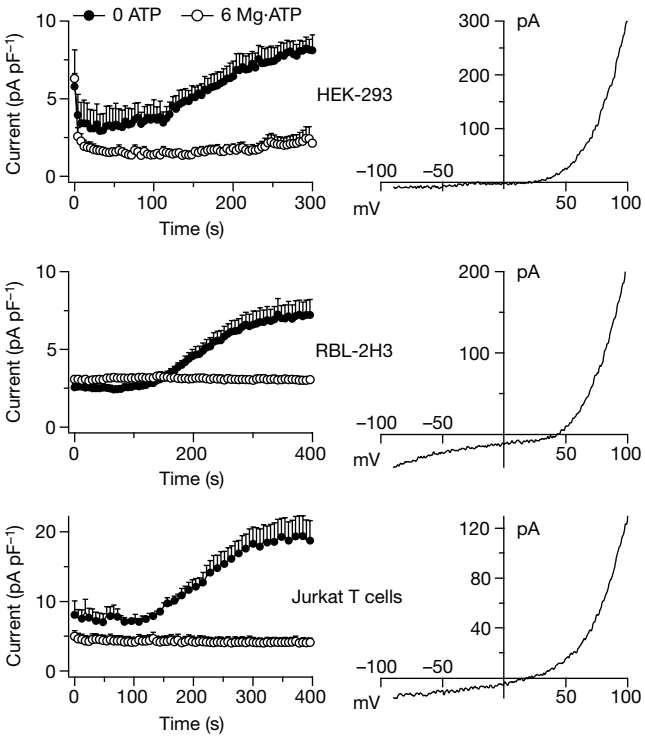

Figure 5 Mg·ATP sensitive conductances with LTRPC7 signature are ubiquitous. Wild-type HEK-293, RBL-2H3 and Jurkat T-lymphocytes were perfused with standard internal solutions supplemented with either 6 mM ATP (open circles; $n = 5$, ± s.e.m.) or no ATP (filled circles; $n = 5$, ± s.e.m.). Under these experimental conditions the store-operated Ca^{2+} current I_{CRAC} contributes a larger proportion of inward currents than when LTRPC7 is overexpressed, accounting for the right-shift in reversal potential.

colleagues also concluded, on the basis of reversal potential measurements, that LTRPC7 is essentially non-selective for monovalent relative to divalent cations. However, as monovalent and divalent ions do not permeate LTRPC7 independently (Fig. 3), the permeation of LTRPC7 at physiological membrane potentials (−40 to −80 mV) is selective for divalent ions, whereas monovalent permeation becomes significant only at rather positive potentials.

In conclusion, we have cloned a member of the LTRPC family of ion channels, designated LTRPC7, and analysed its role in cellular function. Our data indicate that LTRPC7 is an intracellular ligand-gated ion channel whose activation may be linked to cellular energy metabolism through its sensitivity to cytosolic Mg·ATP levels, and that it effectively permeates both Ca^{2+} and Mg^{2+}. As loss of LTRPC7 function would presumably disrupt the coordination of cellular energy production with the homeostasis of these (and possibly other) divalent cations, these functional characteristics plausibly account for the cellular death that occurs in standard cell culture conditions upon deletion of the DT-40 LTRPC7 genes. Furthermore, because of its link to cellular energy metabolism, LTRPC7 may represent a direct mediator of the toxic divalent cation entry that occurs during severe metabolic stress conditions such as hypoxia or hypoglycaemia. □

Methods

Expression analysis

RT–PCR (PCR with reverse transcription) analysis was performed from the indicated human tissue complementary DNA libraries according to the manufacturer's protocols (Life Technologies). For LTRPC7, oligonucleotides used were GTCACTTGGAAACTGG AACC and CGGTAGATGGCCTTCTACTG to produce a 278-base-pair (bp) band. PCR was performed using standard techniques and 30 cycles of 94 °C for 30 s, 55 °C for 30 s, and 72 °C for 60 s. The approximate intensity of the ethidium bromide staining of correct sized bands was estimated by eye to be 1–2+. The LTRPC7 primers used in these reactions were generated from initial expressed sequence tag sequences, and contain a single base pair mismatch at the 5′ end of the primer based on the corresponding region of LTRPC7 sequence obtained from subsequent clones. Multiple tissue northern blots for human tissues and cell lines were obtained from Clontech and all hybridizations were performed according to the manufacturer's protocols. LTRPC7 northern blots were performed using a dUTP-labelled RNA probe generated from a 500-bp fragment corresponding to approximately residues 1,695–2,195 of the human LTRPC7 transcript. The probe was generated using a T7-directed RNA probe synthesis kit from Ambion.

Electrophysiology

HEK-293 cells transfected with the Flag–murineLTRPC7/pCDNA4-TO construct were grown on glass coverslips with DMEM supplemented with 10% fetal bovine serum, blasticidin (5 μg ml^{-1}), and zeocin (0.4 mg ml^{-1}). LTRPC7 expression was induced by adding 1 μg ml^{-1} tetracycline to the culture medium. Whole-cell patch-clamp experiments were performed at 21–25 °C 18–24 h after induction, using cells grown on glass coverslips and kept in a standard modified Ringer's solution of the following composition (in mM): NaCl 145, KCl 2.8, CsCl 10, $CaCl_2$ 1, $MgCl_2$ 2, glucose 10, HEPES·NaOH 10, pH 7.2. In some experiments, nominally $Ca^{2+}$and/or Mg^{2+}-free extracellular solutions or isotonic $CaCl_2$ and $MgCl_2$ solutions (120 mM) were applied by pressure ejection from wide-tipped pipettes. Intracellular pipette-filling solutions contained (in mM): Cs-glutamate 145, NaCl 8, $MgCl_2$ 1, Cs-BAPTA 10, HEPES·CsOH 10, pH 7.2. In some experiments, Cs-glutamate was replaced equimolarly by K-glutamate or choline-chloride. Free [Mg^{2+}]i was calculated by Patcher's Power Tools (http://www.wavemetrics.com/Users/ppt.html). High-resolution current recordings were acquired by a computer-based patch-clamp amplifier system (EPC-9, HEKA). Immediately following establishment of the whole-cell configuration, voltage ramps of 50-ms duration spanning the voltage range of −100 to +100 mV were delivered from a holding potential of 0 mV at a rate of 0.5 Hz over a period of 200–400 s. All voltages were corrected for a liquid junction potential of 10 mV between external and internal solutions when internal solutions contained glutamate. Currents were filtered at 2.3 kHz and digitized at 100-μs intervals. Capacitive currents and series resistance were determined and corrected before each voltage ramp using the automatic capacitance compensation of the EPC-9. The low-resolution temporal development of currents at a given potential was extracted from individual ramp current records by measuring the current amplitudes at voltages of −80 mV or +80 mV.

Full methods for all cloning, construction of expression constructs, SDS–PAGE and immunoprecipitation analyses, and construction of DT-40 cell lines are available as Supplementary Information.

Received 5 December 2000; accepted 23 April 2001.

1. Harteneck, C., Plant, T. D. & Schultz, G. From worm to man: three subfamilies of TRP channels. *Trends Neurosci.* **23,** 159–166 (2000).
2. Ryazanov, A. G. *et al.* Identification of a new class of protein kinases represented by eukaryotic elongation factor-2 kinase. *Proc. Natl Acad. Sci. USA* **94,** 4884–4889 (1997).
3. Romani, A. M. & Scarpa, A. Regulation of cellular magnesium. *Front. Biosci.* **5,** D720–734 (2000).
4. Luthi, D., Gunzel, D. & McGuigan, J. A. Mg-ATP binding: its modification by spermine, the relevance to cytosolic Mg^{2+} buffering, changes in the intracellular ionized Mg^{2+} concentration and the estimation of Mg^{2+} by ^{31}P-NMR. *Exp. Physiol.* **84,** 231–252 (1999).

© 2001 Macmillan Magazines Ltd

5. Runnels, L. W., Yue, L. & Clapham, D. E. TRP-PLIK, a bifunctional protein with kinase and ion channel activities. *Science* **291,** 1043–1047 (2001).

Supplementary Information is available at *Nature*'s World-Wide Web site (http://www.nature.com) or as paper copy from the London editorial office of *Nature*.

Acknowledgements

We thank D. Tani and M. Monteilh-Zoller for technical assistance. This work was funded in part by a Beth Israel Pathology Foundation grant and a BIDMC Fireman Fellowship award to A.M.S., and a NIH grant. A.-L.P. is supported by the German Academic Exchange Service (DAAD).

Correspondence and requests for materials should be addressed to A.M.S. (e-mail: andrewms@u.washington.edu). The GenBank accession numbers for murine and human LTRPC7 cDNA and protein sequences are AY032951 and AY032950, respectively.

ADP-ribose gating of the calcium-permeable LTRPC2 channel revealed by Nudix motif homology

Anne-Laure Perraud*†, Andrea Fleig†‡, Christopher A. Dunn†§, Leigh Ann Bagley‡, Pierre Launay*, Carsten Schmitz*, Alexander J. Stokes*, Qiqin Zhu*, Maurice J. Bessman§, Reinhold Penner‡, Jean-Pierre Kinet* & Andrew M. Scharenberg*‖

** Department of Pathology, Beth Israel Deaconess Medical Center and Harvard Medical School, Boston, Massachusetts 02215, USA*
‡ Laboratory of Cell and Molecular Signaling, Center for Biomedical Research at The Queen's Medical Center and John A. Burns School of Medicine at the University of Hawaii, Honolulu, Hawaii 96813, USA
§ Department of Biology, Johns Hopkins University, Baltimore, Maryland 21218, USA
† These authors contributed equally to this work.

Free ADP-ribose (ADPR), a product of NAD hydrolysis and a breakdown product of the calcium-release second messenger cyclic ADPR (cADPR), has no defined role as an intracellular signalling molecule in vertebrate systems. Here we show that a 350-amino-acid protein (designated NUDT9) and a homologous domain (NUDT9 homology domain) near the carboxy terminus of the LTRPC2/TrpC7 putative cation channel[1] both function as specific ADPR pyrophosphatases. Whole-cell and single-channel analysis of HEK-293 cells expressing LTRPC2 show that LTRPC2 functions as a calcium-permeable cation channel that is specifically gated by free ADPR. The expression of native LTRPC2 transcripts is detectable in many tissues including the U937 monocyte cell line, in which ADPR induces large cation currents (designated I_{ADPR}) that closely match those mediated by recombinant LTRPC2. These results indicate that intracellular ADPR regulates calcium entry into cells that express LTRPC2.

The LTRPC family of putative ion channel proteins[2] has a unique amino-terminal region of 600–700 amino acids that can be divided into 4 smaller sub-regions based on their high level of conservation in one or more family members. Next there is a region of around 300 amino acids that contains the putative pore-forming transmembrane spans, and then a region with predicted coiled-coil character, and finally a C-terminal extension of variable length and unique structure for individual LTRPC members. Figure 1a illustrates the structural elements of LTRPC2, which was originally designated TrpC7 (ref. 1), but was named LTRPC2 in a recently proposed nomenclature[2].

‖ Present address: Department of Pediatrics and Immunology, University of Washington and Children's Hospital and Medical Center, Seattle, Washington 98195-6320, USA.

Whereas northern blotting indicates that LTRPC2 was dominantly expressed in brain (data not shown, consistent with previous reports[1]), polymerase chain reaction after reverse transcription of RNA (RT–PCR) detected LTRPC2 transcripts in many other tissues, including bone marrow, spleen, heart, leukocytes, liver and lung (data not shown). Specificity of the RT–PCR analysis was confirmed by cloning a full-length LTRPC2 transcript from a human monocyte complementary DNA library. On the basis of its unique C-terminal structure, we subsequently cloned a new cDNA from a spleen cDNA library, designated NUDT9. Its expression was detectable by RT–PCR in every tissue analysed, including bone marrow, spleen, heart, leukocytes, liver, lung, kidney, prostate, testis and skeletal muscle (data not shown). The C-terminal region of LTRPC2 and NUDT9 share 50% homology and are also homologous to the *Caenorhabditis elegans* predicted protein EEED8.8 (Fig. 1b). Sequence analysis of NUDT9 revealed the presence of a putative signal peptide/anchor and a Nudix box sequence motif. Nudix boxes are found in a family of diverse enzymes that catalyse the hydrolysis of nucleoside diphosphate derivatives[3]. This motif is highly conserved in EEED8.8, and is present in a less conserved form in the NUDT9 homology region (NUDT9-H) of LTRPC2.

On the basis of the presence of the Nudix box in NUDT9 and the homology between NUDT9 and LTRPC2, we thought that identifying a potential substrate for NUDT9 would provide insight into LTRPC2 function. We therefore expressed NUDT9 in *Escherichia coli*, purified the protein, and screened a series of nucleoside diphosphate derivatives for enzymatic activity. The recombinant protein was a highly specific ADPR pyrophosphatase (yielding AMP and ribose 5-phosphate) with a K_m of 100 ± 10 μM and a V_{max} of 11.8 ± 0.3 μmol min^{-1} mg^{-1} protein. We then expressed the LTRPC2. NUDT9-H in *E. coli* and evaluated its activity towards the same panel of substrates. NUDT9-H had the same specific ADPR pyrophosphatase activity and an identical K_m (100± 10 μM), but a far lower level of activity (V_{max} = 0.1 μmol min^{-1} mg^{-1}). This may be because of the substitution of RIL and QE amino acids in LTRPC2 for the conserved REF triad and EE diad found in the Nudix motifs of NUDT9 and EEED8.8, as these are important for the catalytic activity of other Nudix hydrolases[3]. However, we cannot exclude that the reduced activity of the LTRPC2 NUDT9-H domain relative to that of NUDT9 may be because it is not in its native protein context.

The simplest model to relate NUDT9/NUDT9-H activity to LTRPC2 function is to have LTRPC2 as an ion channel somehow regulated by ADPR. To test this, we used a human embryonic kidney cell line (HEK-293) with tetracycline-regulated transcription of a Flag-tagged LTRPC2 construct. As can be seen in Fig. 2a, in wild-type cells, no transcript was detectable using an LTRPC2-specific probe. After tetracycline induction of cells stably transfected with a textracycline-controlled LTRPC2 construct, substantial expression of an around 6-kilobase (kb) recombinant LTRPC2 transcript was detectable. Similarly, anti-Flag immunoreactive protein of the correct predicted molecular mass was detected in western blots only after tetracycline induction of the stably transfected cells (Fig. 2b). Finally, anti-Flag immunofluorescence indicated that a significant portion of LTRPC2 was localized at or near the plasma membrane (Fig. 2c); this led us to perform patch-clamp analyses of plasma-membrane currents. Without tetracycline induction, ADPR has no detectable effect on plasma-membrane currents (Fig. 2d). Furthermore, in the absence of ADPR in the patch pipette, basal currents in tetracycline-treated cells are the same as in wild-type HEK-293 cells. This indicates that LTRPC2 is not open constitutively under our conditions of standard intracellular solutions. In contrast, after tetracycline induction, large inward and outward currents reversing at 0 mV were induced by 100 μM ADPR (Fig. 2d; Fig. 2e, linear I–V curves at various times of current development). No current activation was observed using 100 μM of a variety of closely related molecules, including NAD^+, cADPR, ATP, ADP,

© 2001 Macmillan Magazines Ltd